The Disilane Chromophore: Photoelectron and Electronic Spectra of Hexaalkyldisilanes and 1,(*n*+2)-Disila[*n.n.n*]propellanes†

Deborah L. Casher,[#] Hayato Tsuji,[‡] Atsushi Sano,[‡] Martins Katkevics,[‡,§] Akio Toshimitsu,[‡] Kohei Tamao,*[,‡] Mari Kubota,[||] Tsunetoshi Kobayashi,[||] C. Henrik Ottosson,[⊥] Donald E. David,[#] and Josef Michl*[,#]

Department of Chemistry and Biochemistry, University of Colorado, Boulder, Colorado 80302-0215, Institute for Chemical Research, Kyoto University, Uji, Kyoto 611-0011, Japan, School of Medicine, Keio University, Hiyoshi-4, Kohoku, Yokohama 223-8521, Japan, and Department of Organic Chemistry, Institute of Chemistry, Box 531, Uppsala University, 751 21 Uppsala, Sweden

Received: November 2, 2002; In Final Form: March 7, 2003

Photoelectron spectra and solution UV absorption and magnetic circular dichroism (MCD) of hexamethyldisilane (**1**), hexaethyldisilane (**2**), hexa-*tert*-butyldisilane (**3**), and the 1,(*n*+2)-disila[*n.n.n*]propellanes [*n* = 4 (**4**) and 5 (**5**)] were measured, as was the linear dichroism (LD) of **3** and **4** partially aligned in stretched polyethylene. The results support the assignment of the lowest energy electronic absorption band of the disilanes **1**−**5** to a doubly degenerate σ_{SiSi}(HOMO) → π^*_{SiC}(LUMO) transition and of the next band, observed in the solution spectra of **2**−**4** and in the gas-phase spectrum of **1**, to a $\sigma_{SiSi} \rightarrow \sigma^*_{SiSi}$ transition. MP2/VTZ optimized geometries of **1**−**5** and ab initio molecular orbital energies (HF/VTZ//MP2/VTZ) and ionization potentials (ROVGF/VTZ//MP2/VTZ) of these disilanes reproduce the reported geometries and the trends observed in the photoelectron spectra, respectively. B3LYP/6-31G(d,p) calculations of the Kohn−Sham orbital energies and TD B3LYP/6-31G(d,p) calculations of transition energies and intensities of **1** as a function of Si−Si bond length suggest that many of the features of the UV absorption spectrum of **3**, including the small energy difference between the two transitions observed and the large extinction coefficient of the band peaking at higher energy ($\sigma_{SiSi} \rightarrow \sigma^*_{SiSi}$), are due to its very long Si−Si bond.

Introduction

Alkylated polysilanes and oligosilanes have drawn much attention because they display unique optical features due to pronounced effects of σ electron delocalization.[1] Considering their fully saturated structure, their UV absorption occurs at remarkably low energies, and this has been attributed[2] to the electropositive character of silicon relative to the lateral substituents. The Si−Si single bond is the fundamental building block for all these and other saturated oligosilane compounds, as well as a prototype for electronic states of other σ bonds, and a thorough understanding of its electronic spectroscopy is therefore desirable.

Surprisingly, little spectroscopic information is available for hexaalkyldisilanes. The photoelectron spectrum of hexamethyldisilane (**1**, Chart 1) has been measured and calculated a long time ago,[3−6] and that of hexaethyldisilane (**2**, Chart 1) has been measured.[6] The isotropic UV absorption spectrum of **1**[7−9] and density functional theory (DFT) calculations of its excitation energies[10] have been reported. Related information can be gleaned from results[11−15] for the parent disilane, Si_2H_6. The most unusual member of the peralkyldisilane series is hexa-*tert*-butyldisilane[16] (**3**, Chart 1), which contains a strikingly long Si−Si bond (2.686 Å, compared to the normal 2.34 Å, observed[17] in **1**). The UV absorption spectra of neither **2** nor **3** appear to have been published.[18] A synthesis of an unusual tricyclic disilane with approximately eclipsed Si−C bonds, 1,6-disila[4.4.4]propellane (**4**, Chart 1), was reported in 1971,[19] and the authors noted that its absorption maximum is significantly red-shifted relative to that of **1**.[7] Unfortunately, the small amounts available inhibited more detailed investigations. Recent synthetic advances[20] provide an opportunity to examine the reactivity and unique structure of **4**. X-ray crystallography revealed a rather short bond length (2.295 Å) and small SiSiC bond angles (105.9°; cf. the usual 110°). A related compound, 1,7-disila[5.5.5]propellane (**5**, Chart 1), has now been prepared in a manner similar to **4**.[20]

CHART 1

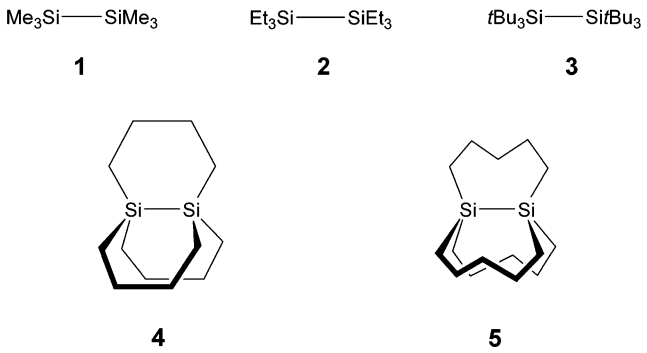

Although convincing arguments in favor of the assignment of the lowest observed UV transition in **1** to valence excitation

† Part of the special issue "George S. Hammond & Michael Kasha Festschrift".

University of Colorado.
‡ Kyoto University.
§ Present address: Latvian Institute of Organic Synthesis, Laboratory of Organometallic Chemistry, 21 Aizkraukles Str., Riga LV-1006, Latvia.
|| Keio University.
⊥ Uppsala University.

10.1021/jp027380q CCC: $25.00
Published on Web 05/01/2003

were presented a long time ago,[21] to this day there is no experimental support for its assignment[10] to a $\sigma\pi^*$ excitation or for the even older conflicting $\sigma\pi^*$[13] and $\sigma\sigma^*$[14,15] assignments for the first transition in the parent Si_2H_6. If the $\sigma\pi^*$ assignment is correct in **1**, it makes this first member of the permethylated oligosilane series quite unique because in permethyltrisilane and all longer peralkylated oligosilanes the first intense observed transition is believed to be due to a $\sigma\sigma^*$ excitation and little is known from experimental observations about $\sigma\pi^*$ excitations.[1,22,23] The purpose of the present paper is to provide an experimental underpinning for an improved understanding of the Si−Si bond as a chromophore, based on a determination of the photoelectron, UV, and magnetic circular dichroism (MCD) spectra of the disilanes **1**−**5** and the linear dichroism (LD) of **3** and **4**.

Experimental and Computational Methods

Materials. Preparative gas chromatography was used to purify a commercial sample of **1** (Aldrich). The disilane **2** was prepared by symmetrical reductive coupling of chlorotriethylsilane followed by distillation.[24] The synthesis of **3** followed the published procedure.[16] Because its UV spectrum differed significantly from all of the others, **3** was subjected to particularly thorough purity checks, including the measurement of ^{1}H, ^{13}C, and ^{29}Si NMR spectra and melting point determination. The disilapropellanes **4**[19,20] and **5**[20] were purified thoroughly by recrystallization from hexanes−ethanol. 3-Methylpentane, the solvent used for absorption and MCD spectra, was purified by passage over a silver nitrate−alumina column.[25]

Photoelectron Spectra. The He(I) photoelectron spectra of **1** and **3** were measured with an instrument described elsewhere[26] at 130 and 142 ± 4 °C, respectively, using argon and xenon as internal standards. Those of **2**, **4**, and **5** were measured with another previously described instrument.[27] Nitrogen gas was used as the internal standard for the calibration of the energy scale, the estimated accuracy of which is ±0.01 eV. The sample inlet and target chamber systems were heated, and their temperature was maintained constant to ±1 °C during the measurements of **4** and **5** at 55 and 47 °C, respectively; **2** was measured at room temperature (22 °C).

Electronic Spectra. UV absorption spectra were recorded with an OLIS RSM 1000 spectrometer at a resolution of 3.8 nm. The spectrometer was calibrated using a holmium oxide filter. Room-temperature spectra of **1**−**5** were taken with ∼10^{-4} M solutions in Suprasil quartz cells with path lengths of 0.2 cm (**1**−**3**) and 1 cm (**4**, **5**). For measurements at 77 K, the solution in a 0.2 cm path length Suprasil quartz cell equipped with a stopcock was immersed in liquid nitrogen in a quartz Dewar flask with Suprasil windows for 5 min before taking the spectrum. The results for 77 K are for samples identical to those run at room temperature and are corrected for a 21.1% solvent contraction.[28] Dipole strengths (*D* terms) were calculated by numerical integration,[29] $D_i = 9.188 \times 10^{-3} \int_i \epsilon \, d\tilde{\nu}/\tilde{\nu}$, in units of square debye.

MCD spectra of **1**−**3** in a 0.1 cm Suprasil quartz cell were run with a JASCO J-720 spectropolarimeter fitted with a 1.5 T electromagnet. MCD spectra of **4** and **5** were recorded in a 1 cm Suprasil quartz cell with a JASCO J-500C spectropolarimeter equipped with a 1.504 T JASCO electromagnet. The magnetic field was parallel to the direction of light propagation and its strength was calibrated against an aqueous solution of $CoSO_4 \cdot 7H_2O$.[30] Between 20 and 100 runs were averaged for each sample run at a resolution of 1 nm, a scan rate of 5−10 nm/min, and a 2−4 s response time. MCD *A* and *B* terms were evaluated in units of $D^2\beta_e$ and $D^2\beta_e/cm^{-1}$, respectively, by numerical integration: $A_i = 33.53^{-1} \int_i d\tilde{\nu}(\tilde{\nu} - \tilde{\nu}_0)[\Theta]_M/\tilde{\nu}$, $B_i = -33.53^{-1} \int_i d\tilde{\nu}[\Theta]_M/\tilde{\nu}$, where $\tilde{\nu}_0$ refers to the wavenumber at the absorption peak and β_e is the Bohr magneton.[29]

The linear dichroism of **3** and **4** in a stretched polyethylene sheet was obtained with a JASCO J-720 spectropolarimeter operating in the LD mode. Polyethylene sheets were cut from a commercial polyethylene bag and cleaned by soaking in chloroform for several hours, then rinsed with fresh chloroform and dried. The purified sheets were stretched to approximately five times their original length. A few drops of a saturated solution of the sample in chloroform were added to one face of the stretched sheet in a covered dish containing a small amount of chloroform. After 1 h, the saturated solution was allowed to evaporate from the sheet, and any crystals remaining on the surface of the sheet were removed by gentle wiping with lens tissue, followed by rinsing with methanol. The stretched sheet was positioned in the spectrometer such that the photoelastic modulator produced light that alternated between polarizations parallel and perpendicular to the stretching direction. A baseline was run beforehand on the same sheet, handled in an identical manner, but without the incorporated sample.

Calculations. Calculations were performed with the Gaussian 98 program[31] with an IBM RS-6000-590 or an HP Exemplar 2000 computer at the University of Colorado at Boulder or with a CRAY T94/4128 or an SGI Origin 2000 supercomputer at the Supercomputer Laboratory of Kyoto University. Molecular orbital contours were visualized with Molden.[32]

The initial geometry of **4** for the optimization procedure was based on its X-ray structure[20] and those of **3** and **5** on structures built with Spartan.[33] Some of the most stable conformers of **2** were identified by a MM3 conformation search, starting with a combination of any two of the seven conformer fragments of the Et_3Si group, which had been calculated[34] to represent stable conformers of Et_3SiH. A rotational conformer search of the resulting disilane around the Si−Si bond was performed to find 19 conformers at energies within 1 kcal/mol of each other.

Geometry optimizations were started at the HF/3-21G(d) level, and frequency analyses were performed at the same level, followed by further optimization at the HF/6-31G(d) and then B3LYP/6-31G(d) levels. MP2/6-31G(d) level geometry optimizations were started from HF/3-21G(d) geometries and followed by MP2 optimization with a 6-311G(d) basis set on silicon, 6-31G(d) on carbon, and 6-31G on hydrogen atoms. This last calculation will be referred to as MP2/VTZ optimization. For the smaller molecules, **1**, **2**, and **4**, we have also calculated the ionization potentials more accurately using the restricted outer valence Green's function (ROVGF/VTZ//MP2/VTZ) electron propagator method[35,36] available in the Gaussian program.

In addition to calculations at the optimized geometries of **1**−**5**, a series of calculations of B3LYP/6-31G(d,p) orbital energies and time-dependent (TD) B3LYP/6-31G(d,p) excitation energies and oscillator strengths of **1** were performed as a function of a rigid stretch of the Si−Si bond (R_{SiSi}), keeping all other geometrical parameters at their equilibrium geometry values.

Results

Geometry Optimization. Si−Si bond lengths and SiSiC angles in the MP2/VTZ optimized geometries of **1**−**5** are listed and compared with the observed values in Table 1. All Si−C bonds had nearly equal lengths of 1.90 ± 0.01 Å. In **1**, the Si−C bonds on the two silicon atoms are perfectly and in **2**

TABLE 1: Geometries and Ionization Potentials (IP) of Disilanes 1−5

	geometry				MO energy,[a] eV HF/VTZ//MP2/VTZ				obsd IP, eV			calcd IP, eV ROVGF/VTZ//MP2/VTZ		
	obsd		MP2/VTZ											
	SiSi, Å	SiSiC, deg	SiSi, Å	SiSiC, deg	σ_1* or π_1* LUMO	σ_1 HOMO	π_1 HOMO − 1	π_2 HOMO − 2	SiSi	SiC	SiC	σ_1	π_1	π_2
1 (D_{3d})	2.340[b]	109.7[b]	2.35	110.22	4.58 (e_u, π_1*)	−9.48 (a_{1g})	−11.35 (e_u)	−11.74 (e_u)	8.7	10.2[c]	10.7[c]	8.4	9.97	10.39
2 (C_1)			2.37	110.65[d]	4.57 (σ_1*)	−9.32	−10.58, −10.59	−10.97, −10.99	8.3	9.4	9.8	8.1	9.13, 9.15	9.54, 9.57
3 (D_3)	2.686[e]	112[e]	2.74	111.61	4.36 (a_2, σ_1*)	−8.85 (a_1)	−9.97 (e)	−10.16 (e)	8.1	∼8.9				
4 (D_3)	2.295[f]	105.9[f]	2.29	105.94	4.71 (a_2, σ_1*)	−8.81 (a_1)	−10.23 (e)	−11.15 (e)	8.0	9.1	9.9	7.6	8.82	9.66
5 (C_3)			2.32	110.38	4.55 (e, π_1*)	−9.18 (a)	−10.43 (e)	−10.70 (e)	8.3	9.3	9.5			

[a] Without empirical corrections. [b] Reference 17. [c] Reference 6 (in our spectrum, these peaks are obscured by Xe). [d] Average of six SiSiC angles. [e] Reference 16. [f] Reference 20.

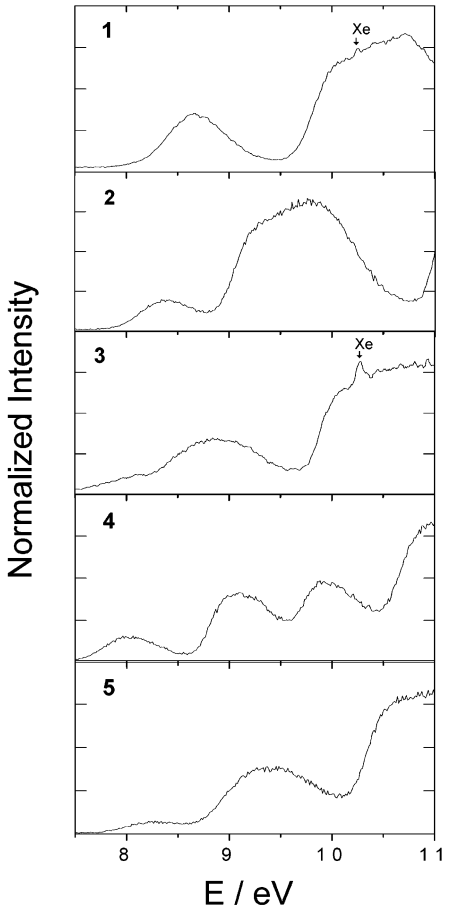

Figure 1. Photoelectron spectra of disilanes **1**−**5**.

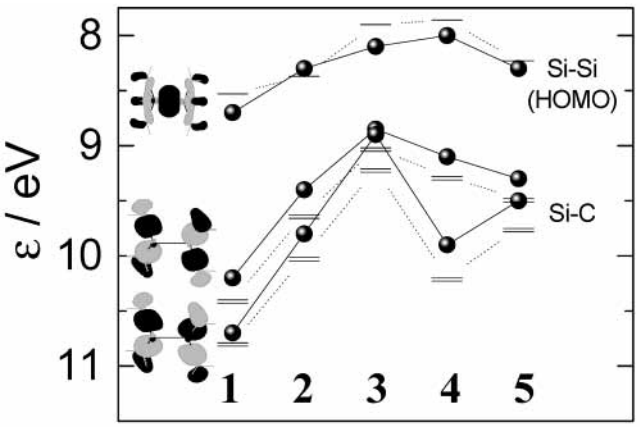

Figure 2. Observed (●) and calculated (−; HF/VTZ//MP2/VTZ, Koopmans' theorem) ionization potentials of disilanes **1**−**5**. All calculated ionization potentials have been reduced by 0.95 eV (see text).

TABLE 2: Electronic Excitation in Disilanes 1−5[a]

	UV abs (RT)			UV abs (77 K)		MCD (RT)		
	$\tilde{\nu}$, cm^{-1}	ϵ_{max}	D^b	$\tilde{\nu}$, cm^{-1}	ϵ_{max}[c]	A[d]	$B \times 10^4$ [e]	$-2A/D$[f]
1	51 900	9 300	9.4	52 300	11 600	3.8	3	−0.81
2	49 800[g]	7 400[g]	5.0[g]	50 600	10 500	1.1	0.75	−0.44
3[h]	48 500 (s)	37 000	13	49 000 (s)	38 000	5.7	21	−0.87
	52 300	43 800	37	51 200	45 900		−4.1	
4	48 100	8 400	8.1	48 400	8 900	3	3.4	−0.74
5	49 600	7 800	8.2	48 800	7 600	3.3	5.5	−0.82

[a] In 3-methylpentane. [b] Dipole strength in square debye. [c] Extinction coefficients at 77 K showed some concentration dependence and are reported for ∼10^{-4} M solutions. [d] A term in $D^2\beta_e$. [e] B term in 10^{-4} $D^2\beta_e$/cm^{-1}. [f] Excited-state magnetic moment in β_e. [g] Gaussian fitting yields ϵ_{max} = 6500 at 49 200 cm^{-1} with the dipole strength reported in the table. [h] Gaussian fitting yields ϵ_{max} = 14 500 at 47 200 cm^{-1} and ϵ_{max} = 44 200 at 52 700 cm^{-1} with the dipole strength reported in the table at RT and ϵ_{max} = 24 600 at 48 200 cm^{-1} and ϵ_{max} = 44 000 at 51 200 cm^{-1} at 77 K. A and B terms for **3** were obtained from the MCD spectrum assuming $\tilde{\nu}_0$ = 47 200 cm^{-1}.

and **3** approximately staggered, while in **4**, they are approximately and in **5** perfectly eclipsed.

Three of the most stable conformers of **2** were found to have almost equal total energies. Results for only one of them, with CCSiSi dihedral angles ag+g+ on one side of the molecule, and ag+g− on the other and a +38° CSiSiC dihedral angle involving the carbon atoms of the anti ethyl groups on the two sides, are shown in Table 1.

Photoelectron Spectra. The photoelectron spectra of **1**−**5** are shown in Figure 1 and summarized in Table 1. The spectra of **1** and **2** are in good agreement with a previous report.[6] In Figure 2, the spectra are compared with $-(\epsilon_i + 0.95$ eV), where ϵ_i are the orbital energies obtained from HF/VTZ//MP2/VTZ calculations. The three low-energy conformers of **2** for which calculations were made gave orbital energies that were identical within 0.01 eV. The constant value of +0.95 eV was added to each orbital energy to correct roughly for the inadequacies of Koopmans' theorem, which overestimates the ionization potentials. For **1**, **2**, and **4**, results of ROVG/VTZ//MP2/VTZ electron propagator calculation of ionization potentials, which goes beyond Koopmans' theorem, are also given in Table 1.

Electronic Spectra. *Absorption.* UV absorption spectra of **1**−**5** in 3-methylpentane are shown in Figure 3 and summarized in Table 2. At room temperature (RT), the lowest energy bands for disilanes **1**−**5** fall between 48 000 and 52 000 cm^{-1}, those of **1** being blue-shifted and those of **3** and **4** red-shifted relative to **2** and **5**. Their maximum extinction coefficients are all around 8000 L mol^{-1} cm^{-1} with the striking exception of the nearly 5 times higher value in the case of **3**. A closer look reveals that in the spectrum of **3** the first band is a shoulder riding on top

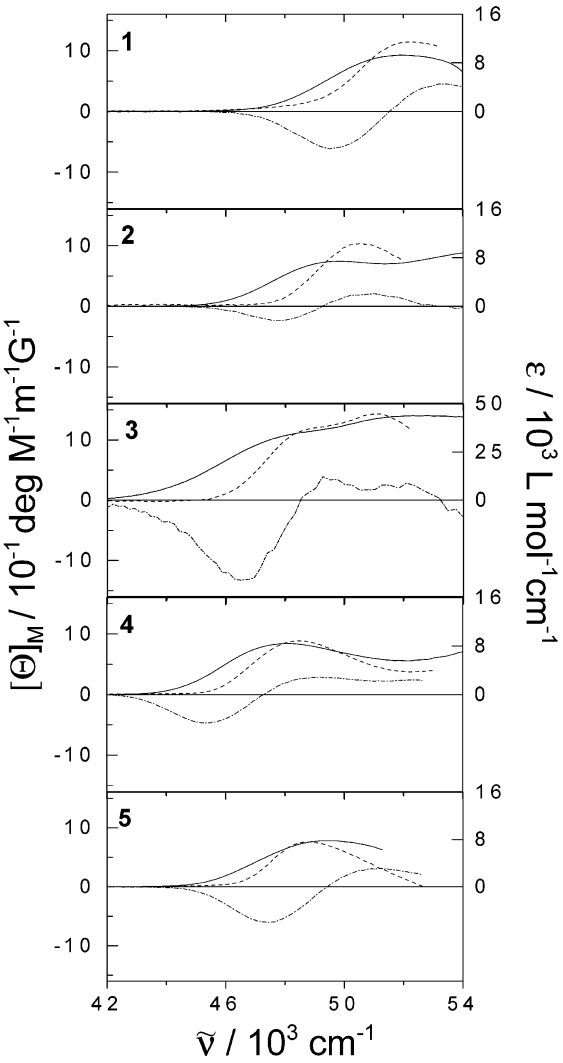

Figure 3. UV (RT —; 77 K − − −) and MCD (RT —·—) spectra of disilanes **1**−**5** in 3-methylpentane.

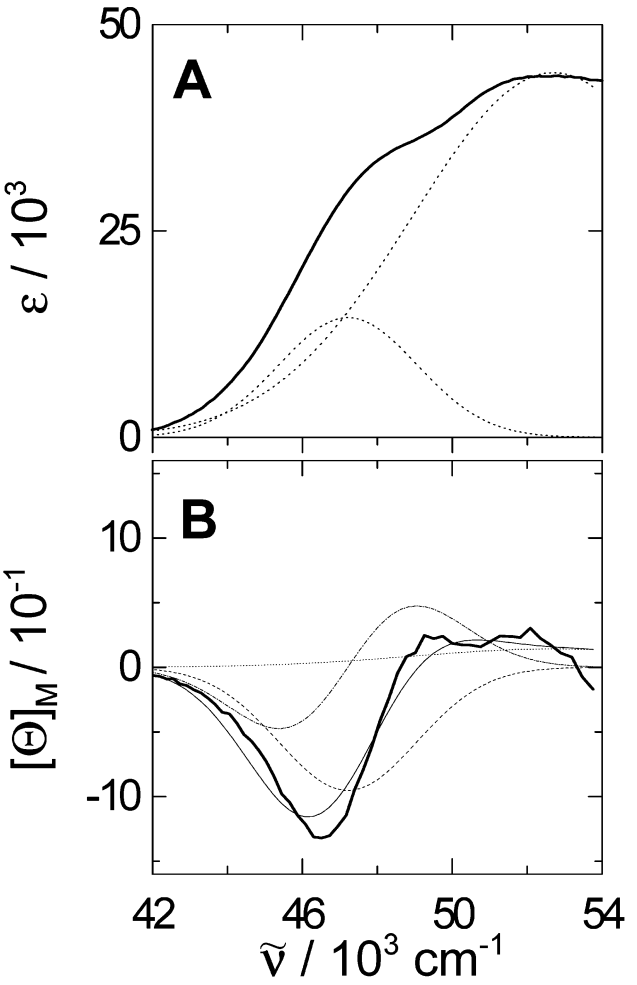

Figure 4. RT (A) absorption of **3** (—) along with Gaussian fit curves (···) and (B) MCD (**—**; *A* term —·—; *B* terms − − −; overall fit —) spectrum of **3**.

of a very broad and much more intense band that starts to rise at lower energies than the first band but peaks at a higher energy, between 52 000 and 53 000 cm^{-1}. Gaussian fitting (Figure 4) suggests that the first band peaks at 47 200 cm^{-1} with an ϵ_{max} of 14 500 and that there is a much broader additional band peaking at 52 800 cm^{-1} with much higher intensity (ϵ_{max} = 44 200). The intensity of the first vertical transition in **3** is thus much more in line with the others than might appear at first sight.

The UV spectra of **2** and **4** also suggest the presence of a second band with a maximum at higher energy just outside our solvent-limited spectral range. Gaussian fitting of **2** gives peaks at 49 100 cm^{-1} (ϵ_{max} = 5600) and 54 300 (ϵ_{max} = 9400). In **4**, the peaks appear to be far enough in energy from one another that no fitting seems necessary. Because we do not observe the absorption maximum in the second transition in **2** and **4**, it is difficult to estimate its intensity reliably, but it appears to be roughly comparable with that of the first transition. This is in striking contrast to the situation in **3** where the intensity of the second transition is 3 times higher than that of the first.

At 77 K, absorption bands are narrower and their peaks are slightly blue-shifted from the RT results, except in the case of **5**, for which the low-temperature absorption peak is somewhat red-shifted. Values reported for the 77 K extinction coefficients were obtained on samples identical with those used for RT measurements. It was observed that decreasing the concentration of the sample by an order of magnitude, to 10^{-5} M, led to higher apparent ϵ_{max} values at 77 K, by as much as a factor of 2. This discrepancy is probably due to limited solubility of the disilanes in the low-temperature glass and aggregation at the higher concentrations. We did not investigate the presumed aggregation phenomenon further and consider the 77 K extinction coefficients to be only qualitatively correct.

Magnetic Circular Dichroism. The room-temperature MCD spectra of **1**−**5** are also shown in Figure 3 and summarized in Table 2. In the case of **1**, **2**, **4**, and **5**, they are dominated by a positive *A* term for the first transition with a superimposed weak *B* term. The MCD signal of the second transition in **2** and in **4** is weak and difficult to evaluate. The MCD spectrum of **3** is also difficult to interpret unambiguously but suggests that the transition peaking at lower energy again has a positive *A* term but now also a relatively large positive *B* term and that the *B* term of the higher energy transition is smaller and negative. This is supported by Gaussian fitting of the spectrum (Figure 4).

The fitting of the absorption spectrum is straightforward, and we assumed that the two band positions and widths that it yielded apply to the MCD spectrum as well. Even with these constraints, there is considerable uncertainty in the MCD fitting shown in Figure 4, and it is conceivable that the *B* term of the first transition is more positive and that of the second transition is more negative than shown.

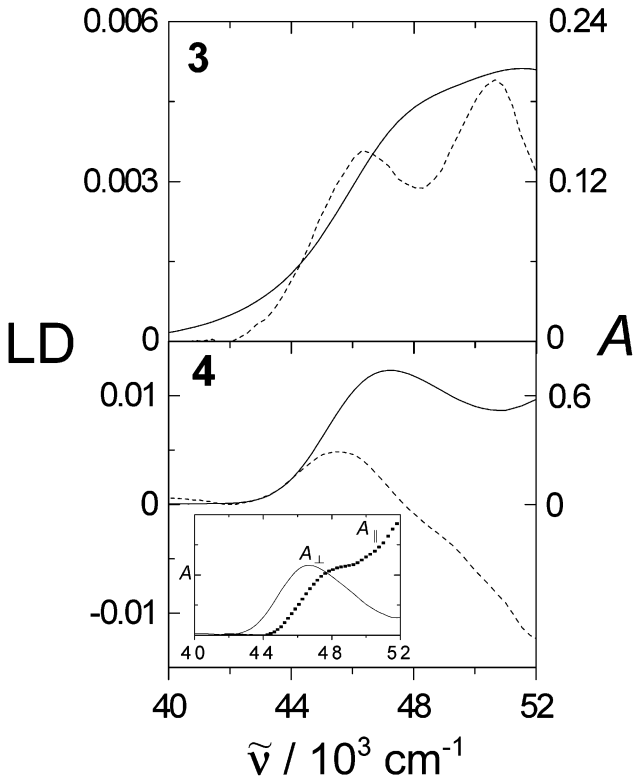

Figure 5. LD (– – –) and absorbance, A (—): (top) results for **3**; (bottom) results for **4**; (inset) reduced spectra in stretched polyethylene ($K_z = 0.337$) with absorbance perpendicular to the 3-fold axis, $A_\perp$ (—), and parallel to it, $A_\parallel$ (■■■).

Linear Dichroism. The presence of two bands in the spectra of **2**−**4** provided an opportunity to determine their relative polarizations by measurement of linear dichroism (LD) in a stretched polyethylene sheet.[37] Because **2** undoubtedly consists of many low-symmetry conformers, each of which could align differently, making interpretation problematic, we have concentrated on the highly symmetrical molecules **3** and **4**. LD spectra (Figure 5) are weak, suggesting that the molecules align only to a small degree, but they are reproducible and demonstrate clearly that the two transitions apparent in the UV spectra are polarized differently.

In **3**, the alignment in stretched polyethylene is such that the transition moment that gives rise to the absorption peak at higher energy is preferentially aligned parallel to the stretching direction (giving a strong positive background in the LD spectrum) and the transition moment responsible for the lower energy shoulder is perpendicular to it (the negative bulge superimposed on the strongly positive LD curve). In **4**, the opposite is true: the LD of the higher energy transition is negative and that of the lower energy transition is positive.

The standard trial-and-error procedure[37] is difficult to apply to find the reduced spectra. This is especially true in the case of **3**, for which lack of clearly distinct spectral features in the linear combinations of absorption and LD curves makes it hard to determine when the shoulder near 48 000 cm^{-1} has been eliminated. The situation is further complicated by the weakness of the LD spectrum and by baseline uncertainties in this spectral region, where polyethylene scatters light strongly. Fortunately, both molecules have a 3-fold rotational axis. Then, only transition moments parallel to the Si−Si bond are possible for nondegenerate allowed excited states (absorbance $A_\parallel$) and only transition intensity in the plane perpendicular to the Si−Si bond is possible for degenerate allowed excited states (absorbance $A_\perp$). Moreover, the axial symmetry of the molecules dictates a relation between the orientation factors K (average squares of direction cosines) of the Si−Si axis and those of any axes perpendicular to it, greatly simplifying the search for the reduced spectra (the axis that aligns best on the average is labeled z and its orientation factor is K_z, while the axis that aligns worst on the average is labeled x and its orientation factor is K_x).[37] Still, we could not reliably determine a unique pair of reduced spectra for **3**. This uncertainty is immaterial for the purpose of relative state symmetry assignment. The reduced spectra of **4** are shown in the inset of Figure 5.

Calculation of the Effects of Si−Si Bond Stretching. In the absence of advanced ab initio results for the excited states of **1**, we attempted a qualitative understanding in terms of DFT. The lowest σ^* and π^* B3LYP/6-31G(d,p) orbital energies of **1** behave quite differently as a function of Si−Si bond length, R_{SiSi} (Figure 6A). The π^* energy does not change much, but the σ^* energy drops steadily as the bond becomes longer. At the same time, the energy of the σ orbital increases as R_{SiSi} grows. For R_{SiSi} equal to 2.3−2.7 Å, the π^* orbital lies below σ^*, and for R_{SiSi} in excess of 2.7 Å, σ^* lies below π^*. TD B3LYP/6-31G(d,p) excitation energies (Figure 6B) exhibit the expected behavior: both the first $\sigma\sigma^*$ and $\sigma\pi^*$ transitions drop in energy with increasing bond length, but $\sigma\sigma^*$ drops much faster. However, for R_{SiSi} smaller than 2.95 Å, the vertical $\sigma\pi^*$ transition remains lower in energy than the vertical $\sigma\sigma^*$ transition. These calculations also show a strong increase in oscillator strength for the $\sigma\sigma^*$ transition with increasing R_{SiSi}, while the oscillator strength for the $\sigma\pi^*$ transition increases only slightly (Figure 6C).

Discussion

Molecular Geometries. The calculated optimized geometries are consistent with the available experimental results, and only the 0.05 Å discrepancy in the Si−Si bond length in the case of **3** is disappointing. The most striking geometrical differences among the disilanes studied are the 2.7 Å long Si−Si bond in **3**, highly unusual compared with the standard 2.34 Å, and the 2.3 Å long Si−Si bonds in **4** and **5**, distinctly shorter than usual. Our results thus provide an opportunity to isolate and examine the effect of bond length on the spectral properties of the Si−Si chromophore because the variation in the other important geometrical parameter, the SiSiC angle, is small. This angle increases by 2° upon going from **1** to **3**. It decreases more significantly, by 4°, upon going from **1** to **4**.

Photoelectron Spectra. Even at the crude level of Koopmans' theorem, ab initio calculations reproduce the qualitative trends observed, except that the lowest calculated ionization potential (IP) of **2** is a little too high (Figure 2). As a result, the reduction in the first IP observed upon going from **2** to **3** is not as much as might have been expected from the immense increase in the Si−Si bond length and as much as has been calculated. We considered the possibility that some of the difficulty might be due to the presence of a large number of conformers of **2**, which could differ slightly in their IPs, but the first peak in its photoelectron spectrum does not appear to be any broader than those of the other disilanes, and the HF/VTZ orbital energies calculated for three low-energy conformers are nearly identical. We conclude that the differences in the first IPs of the important conformers cannot be large.

In agreement with all previous authors, we attribute the first IP to removal of an electron from the σ_{SiSi} orbital (HOMO). The general decrease in this IP with increasing size of the alkyl substituents is readily attributed to the stabilization of the radical

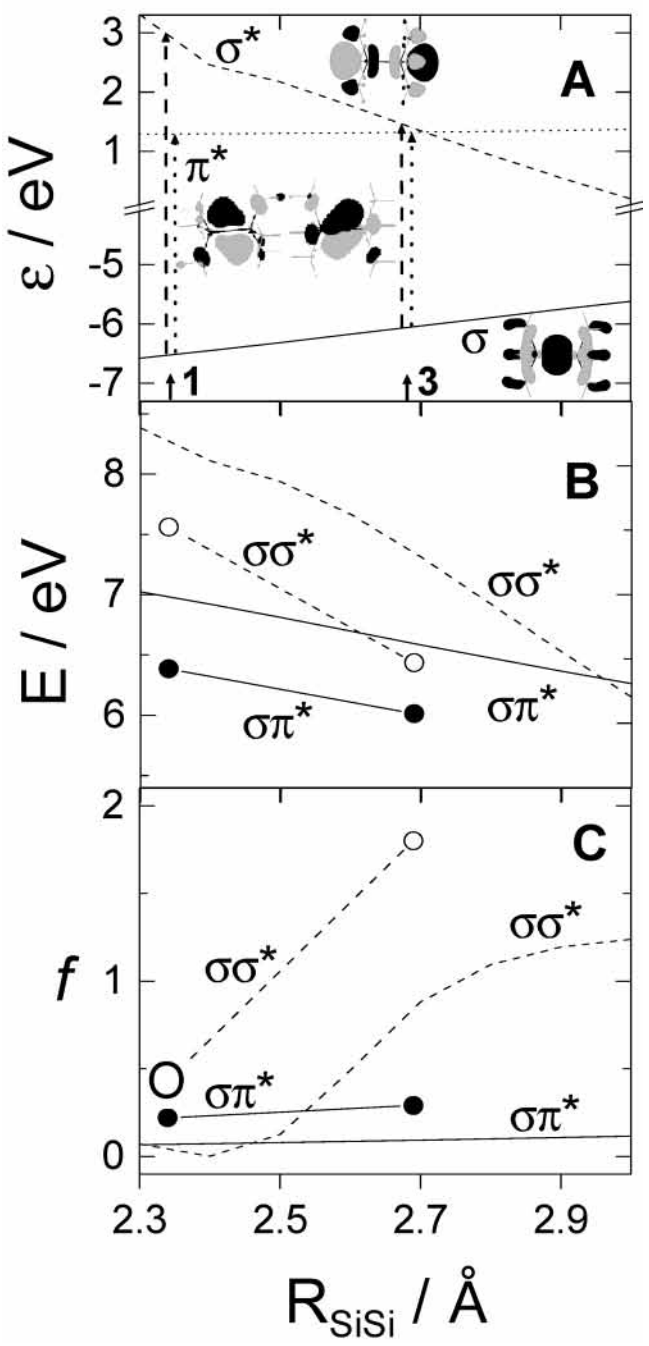

Figure 6. (A) Orbital energy, ϵ, as a function of the Si−Si bond length (R_{SiSi}) in **1** [B3LYP/6-31G(d)]. Contours of molecular orbitals are shown. (B) Excitation energy (E—) of the lowest $\sigma\sigma^*$ and $\sigma\pi^*$ transitions as a function of R_{SiSi} (TD B3LYP/6-31G(d)), and observed transition energies for **1** and **3** (●, $\sigma\pi^*$; ○, $\sigma\sigma^*$). The energy of the $\sigma\sigma^*$ transition in **1** was taken from ref 8. (C) Oscillator strength, f, of the lowest $\sigma\sigma^*$ (− − −) and $\sigma\pi^*$ (—) transitions as a function of R_{SiSi} [TD B3LYP/6-31G(d)], and observed oscillator strengths for **1** and **3** (●, $\sigma\pi^*$; ○, $\sigma\sigma^*$). The oscillator strength of the $\sigma\sigma^*$ transition in **1** was estimated from ref 8.

cation by the increasing polarizable bulk (substituent inductive effect). The ionization of **3** should be less strongly Franck−Condon forbidden than the others. If the positions of peak maxima do not accurately reflect vertical excitation energies, this might be responsible for some of the discrepancies.

We also agree with the previous[4−6] attribution of the broad second spectral band to the second and third IP as due to ionization from two pairs of doubly degenerate combinations of SiC bond orbitals. The separation between the stabilized bonding combination of the two SiC_3 group orbitals and the destabilized antibonding combination is the smallest in **3**, as would be anticipated considering the long Si−Si bond. Its strikingly large value in **4**, 0.8 eV, is similarly attributable to its particularly short Si−Si bond and may be enhanced by the increased p character of its nearly eclipsed Si−C bonds.

Not surprisingly, the electron propagator results agree better with the observed ionization potentials than the negative orbital energies do, even after the empirical correction of the latter (Table 1). Thus, the differences in the lowest ionization potential in the series **1**, **2**, **4** are 0.4 and 0.3 eV; the electron propagator results yield 0.3 and 0.45 eV and Koopmans' theorem 0.16 and 0.51 eV.

Electronic Spectra. The UV absorption spectra of the $R_3Si-SiR_3$ chromophore (Figure 3) are the primary focus of our attention. Comparison with the published[8] vacuum UV spectrum of **1** leaves little doubt that the lowest vertical transition observed in our work for **1**−**5** corresponds to the previously observed lowest transition in the vapor-phase UV spectrum and that the second vertical transition observed presently for **2**−**4** corresponds to the second transition observed in the vacuum UV work. It has been established for a long time[21] that at least the first of these transitions corresponds to a valence excitation, and the persistence of the second transition in solution suggests that it is of valence nature as well. It is probable that weak Rydberg excitations also occur in this region in the gas phase, but we can make no statements about them from our solution work.

Published excited-state calculations[13−15] disagree in the assignment of the first transition in Si_2H_6. DFT calculations for **1**[10,23] attribute the lowest singlet excitation to a degenerate σ (HOMO) to π^* (LUMO) promotion and the next excitation to a nondegenerate $\sigma\sigma^*$ promotion. This requires the presence of an *A* term for the first transition and a perpendicular orientation of the transition moments of the two transitions, exactly as observed in our MCD and LD spectra. The MCD results leave no doubt about the degenerate nature and the $\sigma\pi^*$ assignment of the first transition in **1**−**5** and require little further discussion. The LD results are only available for two of the compounds, **3** and **4**. Although the degree of alignment is clearly small and the LD signal weak, a variation of the degree of dichroism across the accessible region is indisputable and in itself demonstrates that the two transitions are polarized differently (Figure 5). This is sufficient for the assignment of the second vertical transition as $\sigma\sigma^*$, except that as noted below, in some cases a third transition ($\pi\pi^*$) may be contributing as well.

It is of interest to extract the two reduced absorption spectra, $A_{||}$ and $A_{\perp}$. We were unable to do this in an unambiguous manner in the case of **3**. The situation is easier in the case of **4**, for which the degenerate $\sigma\pi^*$ transition, polarized perpendicular to the 3-fold molecular axis, lies at lower energy and is more distinctly separated from the higher transition. Its positive LD then implies that the orientation axis z of **4** in stretched polyethylene is perpendicular to the Si−Si bond direction. Use of standard procedures[37] yields the reduced absorption spectra $(A_y + A_z)/2 = A_{\perp}$ and $A_x = A_{||}$ with the orientation factors $K_y = K_z = 0.337$ and $K_x = 1-2K_z = 0.326$ (inset in Figure 5). Because of baseline uncertainties, the shape of $A_{||}$ is unreliable above ∼50 000 cm^{-1}. It contains a pronounced shoulder at ∼48 000 cm^{-1}, possibly indicating the presence of a second parallel transition in this energy region. Recent TD DFT calculations[23] for **1** indeed predict an intense parallel transition of $\pi\pi^*$ origin at higher energies, in addition to those that we have discussed so far. In **3** − **5**, the π_{SiC} orbitals are significantly

higher in energy than in **1** (Figure 2), and it is conceivable that in these molecules $\pi\pi^*$ excitation contributes in the region observed in our spectra. Higher level calculations are needed before definite assignments will be possible.

In the case of **3**, the relatively narrow $\sigma\pi^*$ transition appears superimposed on the extremely broad band associated with the second transition and produces a negative hump on a broad positive background. This shows that in **3** the orientation axis *z* is parallel to the Si−Si bond direction. Thus, $A_z = A_{||}$ and $(A_x + A_y)/2 = A_\perp$, but the standard trial-and-error reduction procedure is more difficult to apply than was the case for **4**, and its results are not shown.

Irrespective of the uncertainties in the LD and reduced spectra, our results provide strong support for the original assignment of the spectrum of **1**.[10] Although they were obtained on disilanes with alkyl substituents, by extrapolation they make a similar assignment likely for the parent disilane Si_2H_6, in agreement with the calculations reported in ref 13 and in disagreement with those of refs 14 and 15. The similarity of the spectra of **1**−**5** is striking and permits a discussion in terms of a single underlying "$R_3Si-SiR_3$ chromophore". This similarity extends to the values of the dipole strengths and MCD terms of the degenerate first transition and to the magnetic moment of the first excited singlet state, given by $-2A/D$. Its sign is that expected for an excitation from a nondegenerate to a degenerate orbital, and its order of magnitude is as anticipated for a transition that is fundamentally atomic s → p in nature. The significantly lower value of the *A* term and the excited-state magnetic dipole moment in **2** compared to the other disilanes may be related to the presence of numerous conformers in this sample, most of which actually are of low enough symmetry that they do not possess true *A* terms. There could be some partial cancellation of the positive and negative contributions to MCD intensity provided by the various conformers if their transitions occur at slightly different energies.

The only species that stands somewhat apart is **3**, and this is perhaps not surprising in view of its extraordinarily long Si−Si bond. The strong red shift of its $\sigma\sigma^*$ transition can be easily understood in qualitative terms and is in good agreement with our TD DFT calculations. These calculations must be viewed with caution because they do not handle adequately the Rydberg states that are most likely present in the same spectral region as the valence transition of interest. Nevertheless, Figure 6 shows that they qualitatively reproduce the observed variation in both the excitation energy and the oscillator strength of the $\sigma\pi^*$ and $\sigma\sigma^*$ transitions as the Si−Si bond is stretched. However, the absolute values of the calculated excitation energies and oscillator strengths, obtained from the dipole length formula, are clearly overestimated.

The $\sigma\pi^*$ transition is of interest because it represents an extrapolation limit for the poorly understood $\sigma\pi^*$ states of oligosilanes, which have now been detected and assigned in tetrasilanes.[22,23,38] It is in essence a combination of two purely intraatomic transitions involving s to p orbital excitations on the two silicon atoms, and it is not surprising that its intensity is nearly independent of the Si−Si bond length. It is, of course, affected by the weight of the Si 3s orbital in the σ HOMO and of the Si 3p orbital in the π^* LUMO, and these are probably quite although not entirely constant as the Si−Si bond is stretched. The excited-state magnetic dipole moment would be expected to remain nearly constant as well, and it does.

The large intensity of the $\sigma\pi^*$ transition results from the in-phase combination of the transition moments provided by the atomic transition densities on the two Si atoms. This is most simply appreciated by noting that the excitation is from the Si−Si bonding σ_{SiSi} orbital into the most stable and hence also Si−Si bonding π^*_{SiC} orbital (the in-phase combination of SiC_3 group orbitals). In all higher oligosilanes, the lowest $\sigma\pi^*$ excitations will be from the least stable of all of the σ_{SiSi} orbitals, which contains a node at (or near) each Si atom, into one of the most stable π^*_{SiC} orbitals, which contain no or few such nodes. The transition moments contributed by the different Si atoms will be small and will not all add up in phase, and in nearly planar conformers, the low-energy $\sigma\pi^*$ transition will be weak. In this regard, disilane is unique among oligosilanes.

In contrast, the $\sigma\sigma^*$ transition is inherently of interatomic nature, in that its transition density does not integrate to anywhere near zero on each Si atom separately. The transition dipole increases by a factor of 1.15 and the oscillator strength by a factor of 1.32 merely because the Si−Si distance is longer, but the observed and the calculated increase are much larger. This cannot be due to the larger size of the alkyl group because in the calculations methyl groups were used, and must be related to increased atomic charges in the transition dipole. Perhaps the simplistic description of the singlet $\sigma_{SiSi}\sigma^*_{SiSi}$ excited state as the out-of-phase superposition of two contact ion-pair valence bond structures, $R_3Si^+Si^-R_3 \leftrightarrow R_3Si^-Si^+R_3$, which naturally predicts a large oscillator strength, is increasingly correct as R_{SiSi} grows and the bond dissociation limit is approached. If it were not for the existence of Rydberg states, it would indeed be correct at infinite separation.

Conclusion

In summary, the assignment of the lowest vertical transition in the peralkylated disilane chromophore as $\sigma\pi^*$ is secure. It is followed by $\sigma\sigma^*$ (and possibly, $\pi\pi^*$) excitation. It is likely that in Si_2H_6 the situation is the same. It would now be worthwhile to perform high-quality ab initio calculations of excitations in **1**, which would permit an assignment of the higher states observed in vacuum UV, resolve the uncertainties associated with $\pi\pi^*$ excitation, clarify the positions of Rydberg states, and elucidate finer details such as the behavior of the oscillator strengths and excited-state magnetic dipole moments as a function of the Si−Si bond length.

Acknowledgment. Financial support by a Grant-in-Aid from the Ministry of Education, Science, Sports and Culture of Japan (Grants 09239103 and 12CE2005), by the NSF (Grant CHE-0140478), and by a fellowship to H.O. from the Wenner-Gren Foundation is gratefully acknowledged. We thank Professor R. Crespo (University of Valencia, Spain) for useful discussions.

References and Notes

(1) Miller, R. D.; Michl, J. *Chem. Rev.* **1989**, *89*, 1359. West, R. In *Comprehensive Organometallic Chemistry II*; Abel, E. W., Stone, F. G. A., Wilkinson, G., Eds.; Pergamon: Oxford, U.K., 1995; Vol. 2, p 365. Michl, J.; West, R. In *Silicon-Containing Polymers*; Jones, R. G., Ando, W., Chojnowski, J., Eds.; Kluwer Academic Publishers: Dordrecht, The Netherlands, 2000; p 499.

(2) Michl, J. *Acc. Chem. Res.* **1990**, *23*, 127.

(3) Pitt, C. G.; Bursey, M. M.; Rogerson, P. F. *J. Am. Chem. Soc.* **1970**, *92*, 519.

(4) Bock, H.; Ensslin, W. *Angew. Chem., Int. Ed. Engl.* **1971**, *10*, 404.

(5) Szepes, L.; Korányi, T.; Náray-Szabó, G.; Modelli, A.; Distefano, G. *J. Organomet. Chem.* **1981**, *217*, 35.

(6) Mochida, K.; Worley, S. D.; Kochi, J. K. *Bull. Chem. Soc. Jpn.* **1985**, *58*, 3389.

(7) Gilman, H.; Atwell, W. H.; Schwebke, G. L. *J. Organomet. Chem.* **1964**, *2*, 369.

(8) Harada, Y.; Murrell, J. N.; Sheena, H. H. *Chem. Phys. Lett.* **1968**, *1*, 595.

(9) Plitt, H. S.; Balaji, V.; Michl, J. *Chem. Phys. Lett.* **1993**, *213*, 158.
(10) Liu, Z.; Terakura, K.; Abe, S.; Harris, J. F. *J. Chem. Phys.* **1996**, *105*, 8237.
(11) Bock, H.; Ensslin, W.; Fehér, F.; Freund, R. *J. Am. Chem. Soc.* **1976**, *98*, 668.
(12) Nelson, J. T.; Pietro, W. J. *J. Phys. Chem.* **1988**, *92*, 1365.
(13) Balaji, V.; Michl, J. *Polyhedron* **1991**, *10*, 1265.
(14) Gelizé, M.; Dargelos, A.; Márquez, A.; Sanz, J. F. *Chem. Phys.* **1991**, *149*, 333 (continued on p 320).
(15) Crespo, R.; Piqueras, M. C.; Orti, E.; Bredas, J. L. *Synth. Met.* **1991**, *43*, 3457.
(16) Wiberg, N.; Schuster, H.; Simon, A.; Peters, K. *Angew. Chem., Int. Ed. Engl.* **1986**, *25*, 79. Wiberg, N.; Niedermayer, W.; Noth, H.; Knizek, J.; Ponikwar, W.; Polborn, K. *Z. Naturforsch.* **2000**, *55b*, 389.
(17) Beagley, B.; Monaghan, J. J.; Hewitt, T. G. *J. Mol. Struct.* **1971**, *8*, 401.
(18) It has been claimed (*Dictionary of Organometallic Compounds*, 2nd ed., Chapman & Hall: Cambridge, U.K., 1995; Vol. 4, p 4049) that the UV spectrum of hexa-*tert*-butyldisilane was published with the original synthesis (ref 16). However, ref 16 only gives the UV spectrum of hexamethyldisilane.
(19) Tamao, K.; Kumada, M.; Noro, A. *J. Organomet. Chem.* **1971**, *31*, 169.
(20) Toshimitsu, A.; Katkevics, M.; Sano, A.; Asahara, M.; Yamaguchi, S.; Tamao, K. Presented at the 47th Symposium on Organometallic Chemistry, Nagoya, Japan, 2000; Paper A101; unpublished results.
(21) Robin, M. B. *Higher Excited States of Polyatomic Molecules*; Academic Press: New York, 1974; Vol. I, p 305.
(22) Imhof, R.; Teramae, H.; Michl, J. *Chem. Phys. Lett.* **1997**, *270*, 500.
(23) Rooklin, D. W.; Schepers, T.; Raymond-Johansson, M. K.; Michl, J. *Photochem. Photobiol. Sci.*, in press.
(24) Gilman, H.; Shiina, K.; Aoki, D.; Gaj, B. J.; Wittenberg, D.; Brennan, T. *J. Organomet. Chem.* **1968**, *13*, 323.
(25) Murray, E. C.; Keller, R. N. *J. Org. Chem.* **1969**, *34*, 2234.
(26) Fogarty, H. A.; Tsuji, H.; David, D. E.; Ottosson, C.-H.; Michl, J.; Tamao, K.; Ehara, M.; Nakatsuji, H. *J. Phys. Chem. A* **2002**, *106*, 2369 and references therein.
(27) Kubota, M.; Kobayashi, T. *J. Electron Spectrosc. Relat. Phenom.* **1996**, *82*, 61 and references therein.
(28) Murov, S. L.; Carmichael, I.; Hug, G. L. *Handbook of Photochemistry*, 2nd ed.; Marcel Dekker: New York, 1993; p 294.
(29) Klessinger, M.; Michl, J. *Excited States and Photochemistry of Organic Molecules*; VCH Publishers: New York, 1995.
(30) Bötcher, A.; Raabe, G.; Michl, J. *J. Org. Chem.* **1985**, *50*, 5050.
(31) Frisch, M. J. et al. *Gaussian 98*, revision A.6; Gaussian, Inc.: Pittsburgh, PA, 1998.
(32) Schaftenaar, G.; Noordik, J. H. *J. Comput.-Aided Mol. Des.* **2001**, *14*, 123.
(33) *Spartan*, version 4.0; Wavefunction, Inc.: Irvine, CA, 1995.
(34) Fogarty, H. A.; Ottosson, C.-H.; Michl, J. *J. Mol. Struct. (THEOCHEM)* **2000**, *506*, 243.
(35) Niessen, W. von; Schirmer, J.; Cederbaum, L. S. *Comput. Phys. Rep.* **1984**, *1*, 57.
(36) Zakrzewski, V. G.; Ortiz, J. V.; Nichols, J. A.; Heryadi, D.; Yeager, D. L.; Golab, J. T. *Int. J. Quantum Chem.* **1996**, *60*, 29.
(37) Michl, J.; Thulstrup, E. W. *Spectroscopy with Polarized Light*; VCH Publishers: Deerfield Beach, FL, 1995; Chapter 5.
(38) Crespo, R.; Merchán, M.; Michl, J. *J. Phys. Chem. A* **2000**, *104*, 8593.